Journal of Geoscience and Environment Protection, 2025, 13(7), 147-168
https://www.scirp.org/journal/gep
ISSN Online: 2327-4344
ISSN Print: 2327-4336

Hydrochemistry of the Aquifer Systems Associated with the Rio do Rasto Formation in the Municipality of Lages, Santa Catarina, Brazil

Dimitri Tallemberg Soares[1], Manoela Bettarel Bállico[1], Franciéle Schwanck Carlos[2]

[1]Graduate Program in Geology, Federal University of Santa Catarina, Reservoir Geology Laboratory, Florianópolis, Brazil
[2]Federal University of Rio Grande do Sul, Hydraulic Research Institute, Rio Grande do Sul, Brazil
Email: Dimitri.tallemberg@gmail.com

How to cite this paper: Soares, D. T., Bállico, M. B., & Carlos, F. S. (2025). Hydrochemistry of the Aquifer Systems Associated with the Rio do Rasto Formation in the Municipality of Lages, Santa Catarina, Brazil. *Journal of Geoscience and Environment Protection, 13,* 147-168.
https://doi.org/10.4236/gep.2025.137009

Received: May 31, 2025
Accepted: July 20, 2025
Published: July 23, 2025

Abstract

Water is a vital resource for sustaining life and maintaining ecological balance. In recent times, global water demand has increased due to population growth and economic development, raising concerns about the quality of both surface and groundwater. This study focuses on the urban area of Lages, Santa Catarina, Brazil, where the Rio do Rasto Formation—comprising interbedded red sandstones and mudstones deposited from the Late Permian to Triassic periods—predominates. The objective is to assess the hydrochemical characteristics of the aquifer system associated with this formation, utilizing data from existing tubular wells. Data were retrieved from the Groundwater Information System (SIAGAS) and the Water withdrawal permit System of Santa Catarina (SIOUT-SC), which are federal and state-level platforms, respectively, serving as sources of groundwater data in Brazil. The methodology involved hydrochemical interpretation to evaluate the qualitative and quantitative properties of groundwater through its physicochemical parameters. Piper and Schoeller–Berkaloff diagrams were employed to interpret data from four tubular wells, analyzing variables such as calcium, potassium, magnesium, carbonate, bicarbonate, chloride, and nitrate. The Piper diagram indicated that all samples fall within the calcium or magnesium bicarbonate facies. The Schoeller–Berkaloff diagram facilitated the comparison and identification of distinct hydrochemical signatures based on elemental enrichment and depletion patterns. These findings contribute to a better understanding of groundwater quality in the region and underscore the importance of continuous monitoring and data collection to inform sustainable water resource management.

Keywords

Hydrochemistry, Rio do Rasto, Groundwater

1. Introduction

Water is a vital resource for sustaining life on Earth, playing a crucial role in maintaining ecosystem stability and species survival. Population growth and increasing demand for water in economic and industrial development have altered consumption patterns, thereby escalating the need for new, especially potable, water sources (Tubbs Filho, 1994; Hirata et al., 2019). Consequently, concerns regarding water quality—both surface and groundwater—have intensified, reflecting growing interest from researchers, government agencies, and civil society (Menezes et al., 2009).

In Brazil, more than 2.5 million wells reportedly extract approximately 17.58 billion cubic meters of water annually, enough to supply the entire national population for one year (Hirata et al., 2019). Despite this, aquifer management only gained prominence at the turn of the 21st century, when various environmental challenges emerged, including contaminant migration from surface to groundwater, inefficient resource use, increasing social inequality in groundwater access, unsustainable extraction in arid regions, land subsidence due to aquitard compaction, saline intrusion, ecosystem damage, reduced baseflow in dry periods, and insufficient aquifer monitoring (Foster & Chilton, 2003; Edmunds & Smedley, 1996).

Although contaminant migration is generally slow, it has persisted for decades, raising significant concerns. Advances in monitoring technologies have been achieved, yet inadequate groundwater governance remains a challenge. As accessible surface water sources diminish, adopting a cautious and comprehensive approach to groundwater monitoring becomes imperative.

This study focuses on the municipality of Lages in Santa Catarina, Brazil, aiming to characterize the hydrochemical composition of the Rio do Rasto Formation aquifer system. By providing new hydrochemical data for this under-studied formation, the work seeks to contribute to regional groundwater knowledge and inform sustainable resource management.

2. Study Area

The study area is situated within the municipality of Lages, Santa Catarina state, in southern Brazil, covering both the urban perimeter of the city and the Santa Terezinha do Salto district in the rural area (**Figure 1**).

2.1. Geological Context

The study area is located within the Paraná Basin, an intracratonic basin on the South American platform. This basin extends across the Midwest, Southeast, and South regions of Brazil, northern and northwestern Uruguay, parts of Argentina and Paraguay, and has an African counterpart in the Huab Basin of Namibia (Stollhofen et al., 2000; Milani et al., 2007; Holz et al., 2010).

Milani (1997) and Milani et al. (2007) proposed six supersequences in the Paraná Basin, defined by unconformity surfaces spanning several regions. These are:

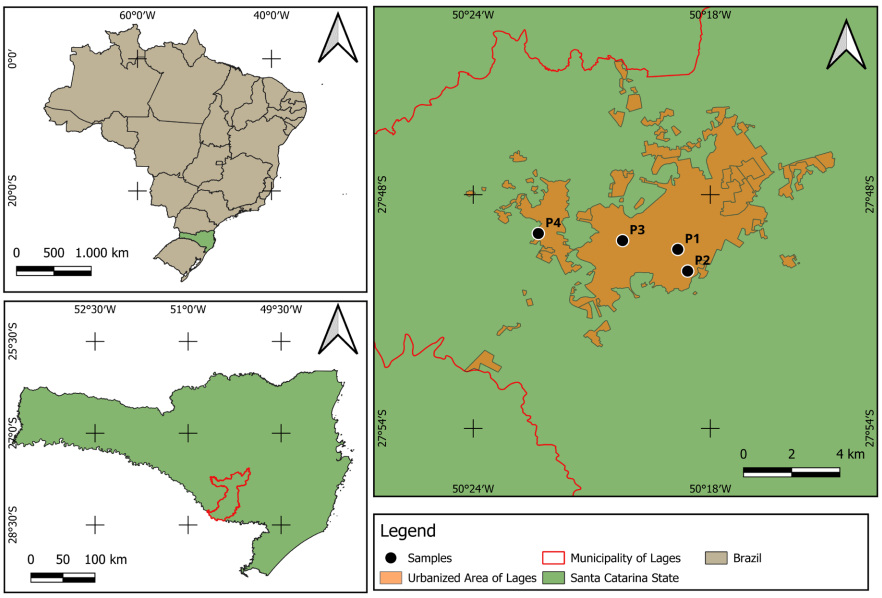

Figure 1. Location map.

Rio Ivaí (Ordovician-Silurian), Paraná (Devonian), Gondwana I (Carboniferous-Eotriassic), Gondwana II (Meso-to Neotriassic), Gondwana III (Neojurassic-Eocretaceous), and Bauru (Neocretaceous). The first three correspond to transgressive-regressive cycles during the Paleozoic, while the latter represent continental sedimentary deposits of the Mesozoic, often associated with igneous rock formations.

The Rio do Rasto Formation, the focus of this study, is part of the Gondwana I supersequence. Gondwana I represents a complete transgressive-regressive cycle, initiated by the marine invasion of the Panthalassa Ocean into the Gondwana supercontinent's interior. This supersequence is the thickest within the Paraná Basin and comprises the Itararé, Guatá, and Passa Dois Groups (Milani et al., 2007). The Rio do Rasto Formation belongs to the Passa Dois Group, which includes the Irati, Serra Alta, Teresina, and Rio do Rasto formations.

Deposited at the end of the Permian, the Rio do Rasto Formation comprises siliciclastic sediments dominated by gray-green, purple, and red shales and siltstones, alongside very fine to medium sandstones in yellow-cream to orange hues (Schneider et al., 1974). It overlies the Teresina Formation in a transitional manner, marked by a shift in fine deposit coloration, fossil assemblages, an increase in sandstone bodies, and a decrease in wavy to lenticular bedding (Rohn, 1994; Warren et al., 2008; Holz et al., 2010). Some authors, however, interpret this contact as discordant due to the abrupt change from Teresina's carbonate deposits to the thick sandstones of the Rio do Rasto (Rohn et al., 2003).

The Rio do Rasto Formation outcrops from northeastern Paraná to southern Rio Grande do Sul, reaching thicknesses up to 400 m and exhibiting a coarsening-upward trend (Schneider et al., 1974; Holz et al., 2010). Originally named by White (1908) after red rock successions near the Rio do Rastro (between Lauro Müller and São Joaquim, Santa Catarina), it was elevated to formation status by

Gordon Jr. (1947), who divided it into the Serrinha Member at the base and the Morro Pelado Member at the top.

The **Serrinha Member** consists of green-gray, brown, burgundy, and red claystones to siltstones, occasionally containing lenses or horizons of marly limestone interbedded with fine gray sandstone lenses (Schneider et al., 1974; Holz et al., 2010; Machado, 2012). These fine sediments typically show planar lamination or wavy and lenticular bedding, without wave or current ripple marks, while sandstones exhibit climbing ripples. Initially described by Rego (1930) in Mallet, Paraná, the member may reach thicknesses between 150 and 250 m. The transition to the Morro Pelado Member is concordant and marked by an increase in sandstone bodies, reflecting a progradational facies pattern. Fine sediments become more reddish upward, indicating progressively more oxidizing conditions.

The **Morro Pelado Member** represents the thickest portion of the Rio do Rasto Formation, ranging from 250 to 300 m in thickness (Schneider et al., 1974; Holz et al., 2010). Defined by Gordon Jr. (1947) based on outcrops near km 19 of the Lauro Müller–São Joaquim highway, it is characterized by increased sandstone occurrence interbedded with purple and red claystones and siltstones. Sedimentary structures in the sandstones include tangential and low-angle cross-beds, fluidized current ripples, while fine sediments display wavy lamination and heterolithic bedding (flaser, wavy, lenticular). Subaerial exposure features and paleosol development are frequently observed.

Although the Rio do Rasto Formation has been extensively studied since the 1930s, this work considers its deposition to occur mainly within the Wordian-Wuchiapingian interval (Middle to Late Permian), despite some studies suggesting extension into the Triassic (Milani, 1997; França et al., 1995). Rohn et al. (2003) indicate that the formation does not reach the Permo-Triassic boundary but records increasing aridification toward the Paleozoic's end, potentially contributing to the Permo-Triassic extinction. **Figure 2** shows the main lithologies identified in the study area.

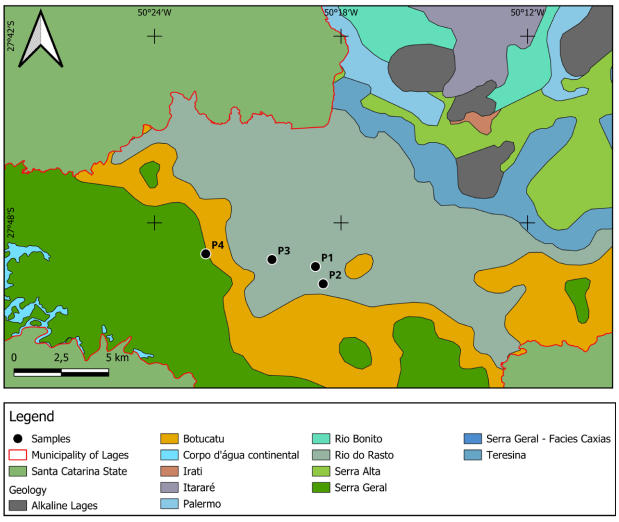

Figure 2. Geological map.

2.2. Hydrogeological Context

The municipality of Lages is located within the Hydrographic Region of the Lages Plateau, which is the largest hydrographic region in terms of area in the state of Santa Catarina (Figure 3). This region encompasses two main basins: the Canoas River Basin and the Pelotas River Basin. The Canoas River Basin includes tributaries such as the Caveiras, Marombas, Correntes, and Lava Tudo rivers. The Pelotas River, which serves as a natural boundary between Santa Catarina and Rio Grande do Sul states, has major tributaries including the Invernadinha, Lava Tudo, and Pelotinhas rivers. The confluence of the Canoas and Pelotas rivers forms the Uruguay River, which eventually flows into the Río de la Plata estuary (State Secretariat for Sustainable Economic Development, 2017). However, the study area is exclusively situated within the Canoas River Basin.

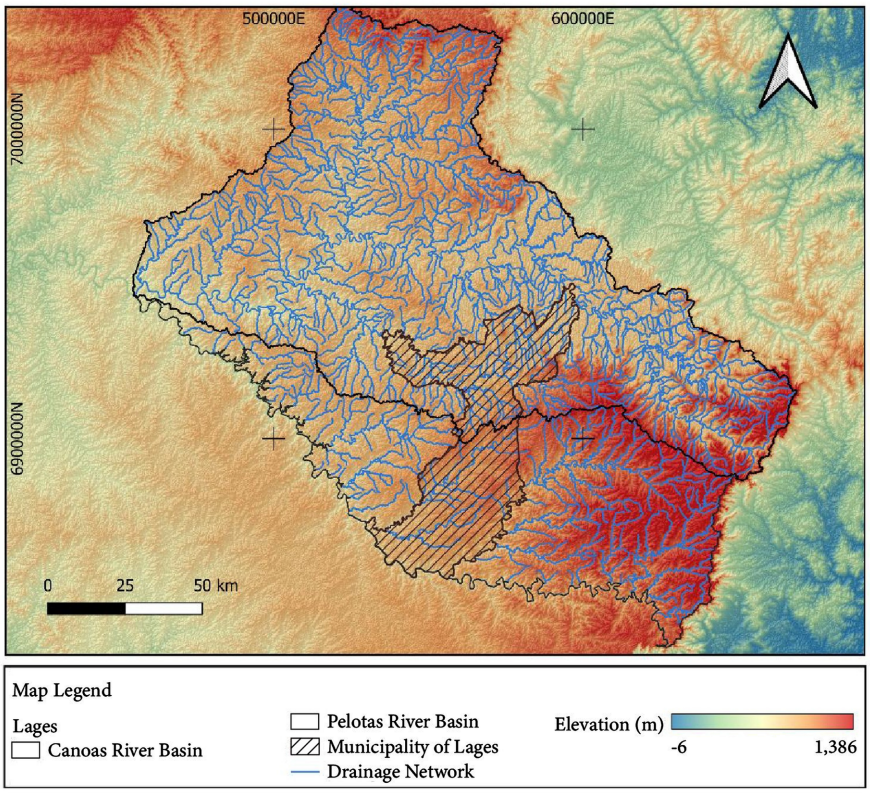

Figure 3. Hydrogeological map.

Following the delimitation of the Hydrographic Region and Basin, the classification of hydrogeological domains within Lages can be addressed. The municipality exhibits three hydrogeological domains: Crystalline, Volcanic, and Sedimentary Basin domains. The study area specifically corresponds to the Paraná Basin hydrogeological subdomain, also referred to as the Paraná Hydrogeological Province. This province is characterized by general similarities in the main groundwater occurrences, primarily controlled by lithology, structure, and tectonics (Tolman, 1937). The Paraná Province is known for its high aquifer productivity, with

the greatest groundwater potential found in extensive Mesozoic sedimentary sequences that include lithostratigraphic units such as the Botucatu, Pirambóia, Rio do Rasto formations, among others. The Serra Geral Formation is also notable within this context, exhibiting characteristics of a fractured aquifer system (Soares et al., 2008). **Figure 3** illustrates the hydrographic basins within the study area, highlighting the Canoas and Pelotas basins, with the municipality of Lages delineated by hatching.

According to Machado (2012), who conducted a hydrogeological characterization of Santa Catarina state, the northern portion near the Paraná border features extensive outcrops of the Rio do Rasto unit between the municipalities of Canoinhas and Porto União. A well drilled in Porto União reached a depth of 120 meters and yielded a flow rate of 8.8 m^3/h with a specific capacity of 0.39 m^3/h/m, values considered representative of regional average well performance. Regarding water quality, total dissolved solids rarely exceed 150 mg/L, and pH values range from acidic to slightly alkaline.

Between Monte Castelo and São Cristóvão do Sul municipalities, the Rio do Rasto unit occurs in topographically unfavorable hydrogeological settings, with steep and rugged terrain that limit infiltration and water storage capacity. In these areas, water use is primarily restricted to natural springs.

From São Cristóvão do Sul to near Bom Retiro, significant outcrops of the aquifer portion of the unit occur, influenced by the alkaline intrusion of Lages and tectonic activities related to the uplift of the Serra do Mar. This region, encompassing the study area of this research, offers favorable conditions for groundwater extraction through moderately deep tubular wells. However, hydrogeological potential varies considerably, as illustrated by local well data: in Otacílio Costa, a 264 m deep well yielded 10 m^3/h with a specific capacity of 0.28 m^3/h/m; in the Lages Industrial District, a 172 m well penetrating the lower productivity Botucatu Formation produced 31.6 m^3/h, a specific capacity of 1.09 m^3/h/m, and a static water level of 54.15 m; in Urubici, a 112 m well reached 15 m^3/h with a specific capacity of 1.70 m^3/h/m. Water quality in this region meets public, agricultural, and industrial use standards, with pH ranging from acidic to slightly alkaline, though iron concentrations may exceed regulatory limits.

South of Bom Retiro toward the carboniferous region, the Rio do Rasto unit returns to steep Serra do Mar slopes, where rugged relief again limits recharge and water storage. Here, the unit's topography reaches elevations between 1,000 and 1,300 meters, mostly in unpopulated areas. From the carboniferous zone southward to the border with Rio Grande do Sul, the Rio do Rasto unit gradually descends towards sea level, overlain by Cenozoic marine sediments. In this area, the unit presents the most favorable hydrogeological conditions in Santa Catarina. Though multilayered, it is primarily composed of the more sandy Morro Pelado Member, whose productivity may be significantly influenced by fracturing. For example, a well drilled in urban Jacinto Machado reached 104 m depth, yielding 25 m^3/h with a drawdown of 9 m and a specific capacity of 2.77 m^3/h/m, charac-

terizing it as one of the highest potential areas of the unit in the state.

In deeper confined zones of the unit, notable tubular wells were drilled in Treze Tílias and São João do Oeste, showing excellent hydraulic properties. In Treze Tílias, a 750 m deep well (with 255 m in the Rio do Rasto unit) recorded a flow rate of 95.7 m^3/h and a specific capacity of 1.70 m^3/h/m. Hydrodynamic parameters—storage coefficient of 9.7×10^{-4}, transmissivity of 49.87 m^2/day, and hydraulic conductivity of 0.24 m/day—confirm the confined nature of the aquifer. At São João do Oeste, a 1376 m well (101 m in the Rio do Rasto unit) yielded 106.98 m^3/h with a specific capacity of 1.29 m^3/h/m, an elastic storage coefficient of 3.5×10^{-4}, transmissivity of 39.80 m^2/day, and hydraulic conductivity of 0.37 m/day. These parameters are considered representative of the unit and demonstrate its high hydrogeological potential.

Regarding water chemistry, a trend of deterioration is observed with increasing depth. The Treze Tílias well showed total dissolved solids ranging from 306 to 357 mg/L and pH between 9.5 and 9.78, indicating high alkalinity. Temperatures ranged from 29.5˚C to 32.0˚C. In São João do Oeste, salinity varied between 3,834 and 4,425 mg/L with pH values from 7.3 to 7.7, suggesting possible mixing with waters from other Permian aquifers. The temperature recorded in this well, influenced by its great depth, reached 50.0˚C.

3. Methods and Materials

To develop the database, information was collected from various platforms, including the Groundwater Information System (SIAGAS) and the Water withdrawal permit System of Santa Catarina (SIOUT-SC)[1], as well as scientific articles related to the topics addressed. The sampled wells are located on both public and private properties and serve a range of purposes, including human consumption, sanitary use, cleaning, landscape irrigation, domestic water supply, agricultural irrigation, vehicle washing, and laundry services.

In this study, eight water samples were collected from four tubular wells during two separate campaigns. The first sampling campaign was conducted in the winter of 2023, and the second took place in the summer of 2024. This temporal division aimed to observe the variation in the concentration of the sampled compounds across different seasons, as elements tend to show higher concentrations during dry periods due to reduced water recharge, contrasting with wetter periods.

The nomenclature used to reference each well was: P1, P2, P3, and P4. Each well serves a distinct purpose: P1 is used exclusively for laundry activities; P2 is designated for domestic water supply, cleaning, urinal flushing, and landscaping; P3 is used for domestic water supply, cleaning, urinal flushing, and irrigation; and P4 serves commercial purposes, including human consumption and vehicle washing.

[1]Although the abbreviations SIAGAS and SIOUT-SC may not be immediately meaningful in English, they derive from the original Portuguese names Sistema de Informações de Águas Subterrâneas (Groundwater Information System) and Sistema de Outorga de Santa Catarina (Santa Catarina Water Withdrawal Permit System), respectively.

Table 1 presents the wells selected for this study, or nearby wells, based on the information available from the aforementioned platforms.

Table 1. Details of selected or nearby wells.

Name	Coordinates UTM (north/south)	Coordinates UTM (east/west)	Depths (m)	Lithology	Screened Intervals (m)
JB815	6923026	561593	130	Argillaceous sandstone	0 a 030
JB819	6924235	562896	100	Medium(-grained) sandstone	6 a 100
JB826	6923222	565993	136	Medium(-grained) sandstone	2 a 136
JB828	6922927	568202	36	Shale	2.5 a 36
JB831	6922701	565087	60	sandy clay	3 a 60
JB832	6922395	567068	100	Argillaceous sandstone	15 a 100
JB832	6922395	567068	100	Argillaceous sandstone	0 a 100
JB833	6924007	566932	80	Argillaceous sandstone	4 a 80
JB836	6928197	566838	170	Argillaceous sandstone	3 a 170
JB863	6922546	565508	100	Argillaceous sandstone	30 a 100

3.1. Sampling

Samples were collected using sterilized 300 mL polyethylene bottles with screw caps. When necessary, samples were preserved with nitric acid and kept refrigerated without reaching the freezing point. In locations with difficult direct access to wells, samples were collected from pipelines directly connected to the wells or water tanks prior to treatment.

After collection, samples were stored in thermal boxes with ice to maintain low temperatures during transportation to the laboratories at the Federal University of Santa Catarina (UFSC). At UFSC, samples were distributed to three laboratories: the Integrated Environmental Laboratory (LIMA), where calcium, magnesium, bicarbonate, electrical conductivity, pH, and total dissolved solids were analyzed; the Atomic and Mass Spectrometry Laboratory (LEMA), responsible for nitrate, nitrite, chloride, sulfate, phosphate, and fluoride ions analysis; and the Central Analysis Laboratory, where sodium and potassium levels were quantified.

3.1. Hydrochemical Analysis

The hydrochemical analysis in this study is based on the interpretation of the following parameters: hydrogen potential (pH), electrical conductivity (EC), total dissolved solids (TDS), bicarbonate (HCO_3^-), carbonate (CO_3^{2-}), total iron (Fe^{2+} and Fe^{3+}), calcium (Ca^{2+}), magnesium (Mg^{2+}), sodium (Na^+), potassium (K^+), sulfate (SO_4^{2-}), chloride (Cl^-), nitrite (NO_2^-), nitrate (NO_3^-), and fluoride (F^-). Based on these parameters, the hydrochemical character was identified using Piper and Schoeller-Berkalof diagrams.

3.2. Parameter Analysis Methods

3.2.1. pH

The pH measurement was performed using a portable pH meter by the brand KASVI. The device consists of two conjugated electrodes: an indicator electrode and a reference electrode. The reference electrode maintains a constant potential, while the indicator electrode acquires the sample's pH by comparison with the reference.

3.2.2. Electrical Conductivity (EC)

The method used to determine EC employed a bench conductivity meter, model BelW12D, which consists of a Wheatstone bridge and a conductivity cell to measure the sample's electrical resistance.

3.2.3. Alkalinity

The analysis method depends on the sample pH: if pH is above 8.3, phenolphthalein is used; if below 8.3, methyl orange is applied. In this study, methyl orange was used for the collected samples.

3.2.4. Hardness

Calcium (Ca^{2+}) and magnesium (Mg^{2+}) ions in the solution form a wine-red complex with the eriochrome black T dye at pH 10.0 ± 0.1. Adding EDTA to the colored solution results in a stable, non-dissociated complex with Ca^{2+} and Mg^{2+}, displacing the dye. When enough EDTA is added to complex all calcium and magnesium, the solution turns back to the dye's original blue color, indicating the titration endpoint.

3.2.5. Total Iron

This parameter was analyzed using a HACH DR3900 spectrophotometer via the 1,10-phenanthroline method, which forms a complex ion with a 3:1 ratio between 1,10-phenanthroline and Fe^{2+}. The absorbance was measured at 510 nm wavelength.

3.2.6. Major Anions

Analysis was performed by chromatography, a method for separating mixture components for identification or quantification based on their interaction with the stationary and mobile phases. In this study, chromatography was used exclusively to identify anions: F^-, Cl^-, NO_2^-, NO_3^-, and SO_4^{2-}. An ion chromatograph (MODEL, DIONEX) equipped with an automatic autosampler (AD-SV), sample flow splitter, two pumps (gradient and isocratic), two electrochemical eluent generators, analytical and guard chromatographic columns, an automatic injector, two conductivity detectors (DC-5000), and a UV detector (deuterium-tungsten VWD) was used. Calibration curves, equations, correlation coefficients, and typical chromatograms were obtained from diluted commercial standard solutions. The analysis procedure consists of passing the liquid sample (mobile phase) through a column containing ion-exchange resin (stationary phase). Ion separa-

tion occurs by ion exchange with resin functional groups. Ionic concentrations are determined by integrating the peak area in the chromatogram.

3.2.7. Major Cations

The cation analysis was conducted by atomic absorption spectrometry (AAS), which measures the absorption of electromagnetic radiation intensity from a primary radiation source by gaseous atoms in the ground state. The two most common atomizers are graphite furnace and flame; the flame atomizer was used in this study. The sample is directly measured by comparing it with a metal calibration curve. The sample is subjected to an air-acetylene flame where the matrix burns and the metal is ionized. The analyte absorbs part of the photon beam emitted by a hollow cathode lamp of the same metal. The difference between initial and final radiation intensity is measured by the detector. This method was used to analyze Mg^{2+}, Na^{+}, and K^{+} ions.

A summary table (**Table 2**) lists the parameters and their respective analytical methods. It is important to note that the methods employed have a quantification limit of 0.1 mg/L and a detection limit of 0.03 mg/L. Although the margin of error may vary, the average error is approximately 0.05 mg/L, based on calibration curves with a coefficient of determination (R^2) of 99%.

Table 2. Summary of the sampled ions and methods of analysis.

Parameter	Analytical Method
Mg^{2+}, Na^{+} e K^{+}	Atomic Absorption Spectrometry (AAS)
F^{-}, Cl^{-}, NO_2^{-}, NO_3^{2-} e SO_4^{2-}	Ion Chromatography (IC)
Fe^{2+} e Fe^{3+}	Total Iron by Spectrophotometry (1,10-phenanthroline method)
HCO_3^{-} e CO_3^{2-}	Alkalinity by Acid-Base Titration
Ca^{2+}	Complexometric Titration (Hardness)

3.3. Ionic Balance (I.B.)

According to Fenzl & Ramos (1986), validating hydrochemical data requires the calculation of the ionic balance, which helps identify potential analytical errors in each sample. To ensure consistency and reliability in hydrochemical interpretations, the sum of cations (in meq/L) should be approximately equal to the sum of anions (in meq/L) for the same sample, within an acceptable error range.

Conversion of ion concentrations from mg/L to meq/L was performed using the conversion factors presented in **Table 3**, as proposed by Feitosa et al. (2008). These constants are derived from Equation (1), which considers the ion valence and atomic weight.

$$\frac{\text{meq}}{\text{L}} = \frac{\frac{\text{mg}}{\text{L}} x \text{ valence}}{\text{atomic weight}} \quad (1)$$

Table 3. Levels of the ions analyzed separately into winter and summer.

Winter												
Sample	Sodium	Potassium	Calcium	Magnesium	Chloride	Bicarbonate	Sulfate	EC	pH	Nitrate	Fluoride	Nitrite
P1	1.900	0.420	7.200	1.814	0.441	18.000	3.116	46.600	9.300	0.926	0.830	<0.03
P2	20.140	3.060	58.400	9.503	1.922	188.000	1.631	298.000	7.500	0.591	0.110	<0.03
P3	6.640	3.040	88.800	20.916	9.369	222.000	6.485	473.000	7.000	5.431	0.251	<0.03
P4	7.850	5.050	63.200	11.358	1.042	158.000	1.446	245.000	7.200	0.139	0.122	<0.03
Summer												
Sample	Sodium	Potassium	Calcium	Magnesium	Chloride	Bicarbonate	Sulfate	EC	pH	Nitrate	Fluoride	Nitrite
P1	1.520	0.357	11.200	2.700	6.220	322.000	84.430	1217.000	8.500	0.100	1.950	<0.03
P2	16.112	2.601	56.000	11.160	1.880	112.000	1.550	328.000	8.600	0.640	0.120	<0.03
P3	5.312	2.584	69.600	20.155	10.020	124.000	6.630	471.000	8.200	6.170	0.190	<0.03
P4	6.280	4.293	51.200	12.025	0.130	84.000	0.920	242.000	7.800	0.160	0.030	<0.03

The ionic balance calculations were performed using the Qualigraf software, which implements two distinct equations—one proposed by Custódio & Llamas (1983) and the other by Logan (1965).

The equation derived from Custódio & Llamas (1983) is illustrated in **Figure 4**. In this approach, electrical conductivity is considered a key factor influencing the permissible range of analytical error in the ionic balance.

Ionic Balance No 1

Based on the Practical Error (PE), defined by Custódio & Llamas (1983):

$$PE\ (\%) = \left| \frac{r\,\Sigma anions - r\,\Sigma cations}{r\,\Sigma anions + r\,\Sigma cations} \right| \times 200$$

The theoretical error is the maximum allowed PE, in terms of electrical conductivity (EC), as shown:

Electrical Conductivity (µS/cm)	50	200	500	2.000	>2.000
Allowed error (%)	30	10	08	04	<04

Figure 4. Practical error based on Custódio and Llamas (1983).

For the equation proposed by Logan (1965), see **Figure 5**.

Ionic Balance Nº 2

Based on the Practical Error (PE), defined by Logan (1965):

$$PE\ (\%) = \left| \frac{r\,\Sigma anions - r\,\Sigma cations}{r\,\Sigma anions + r\,\Sigma cations} \right| \times 200$$

The theoretical error is the maximum allowed PE, taking into account the ion values, as shown:

∑cation or ∑anions	<01	01	02	06	10	30	>30
Allowed error (%)	15	10	06	04	03	02	01

Figure 5. Practical error based on Logan (1985).

This method also evaluates the accuracy of the ionic balance, albeit using a dif-

ferent approach for calculating the relative error between the total concentrations of cations and anions. Like the method of Custódio & Llamas (1983), it is commonly applied in hydrochemical assessments and provides a complementary validation tool for the consistency of analytical results.

Samples exhibiting values beyond the acceptable error threshold should not be disregarded, as they may indicate analytical or calculation errors, the presence of minor ions in significant concentrations, trace elements, or even poorly mineralized waters such as rainwater. This consideration is particularly relevant given that only the major ions Na^+, K^+, Ca^{2+}, Mg^{2+}, NO_3^-, Cl^-, SO_4^{2-}, HCO_3^-, and CO_2 were analyzed in this study. According to Fenzl & Ramos (1986), standard analytical methods tend to be less accurate at low ionic concentrations, which may lead to relatively high calculated errors that do not necessarily imply a true analytical or computational mistake.

3.4. Piper Diagram

According to Hounslow (2018), four key interpretations can be drawn from the use of the Piper diagram: water types, precipitation or dissolution processes, mixing trends, and ion exchange mechanisms. The diagram plots the major ionic constituents cations (Na^+, K^+, Ca^{2+}, and Mg^{2+}) and anions (NO_3^-, Cl^-, SO_4^{2-}, HCO_3^-, and CO_3^{2-}) to classify groundwater types within an aquifer and to distinguish hydrochemical facies (Custódio & Llamas, 1983).

3.5. Schoeller-Berkaloff Diagram

The Schoeller-Berkaloff diagram is a semi-logarithmic plot in which ion concentrations are expressed in meq/L. This graphical method enables the comparison of associated ions, differentiation between hydrochemical water types, and analysis of the variability among dominant ions across multiple samples.

4. Results and Discussion

The data concerning ion concentrations in the water samples collected during the analyzed periods are presented in **Table 3**, with concentrations expressed in mg/L. **Figure 6** and **Figure 7** illustrate the 24-hour accumulated rainfall recorded at the Lages meteorological station for the months in which sampling occurred: August 2023 (winter) and January 2024 (summer), with totals of 74.4 mm and 193 mm, respectively.

It was observed that precipitation during the winter sampling period was concentrated in the second week of August, with the highest daily peak reaching approximately 24 mm. During the summer campaign, several days experienced moderate to heavy rainfall events, with daily accumulations exceeding 30 mm, and the highest peak reaching approximately 60 mm.

Based on the collected data, two tables were developed to support further analyses: one for descriptive statistical analysis (**Table 4**) and another for ionic balance calculations (**Table 5**). **Table 4** summarizes the statistical parameters obtained

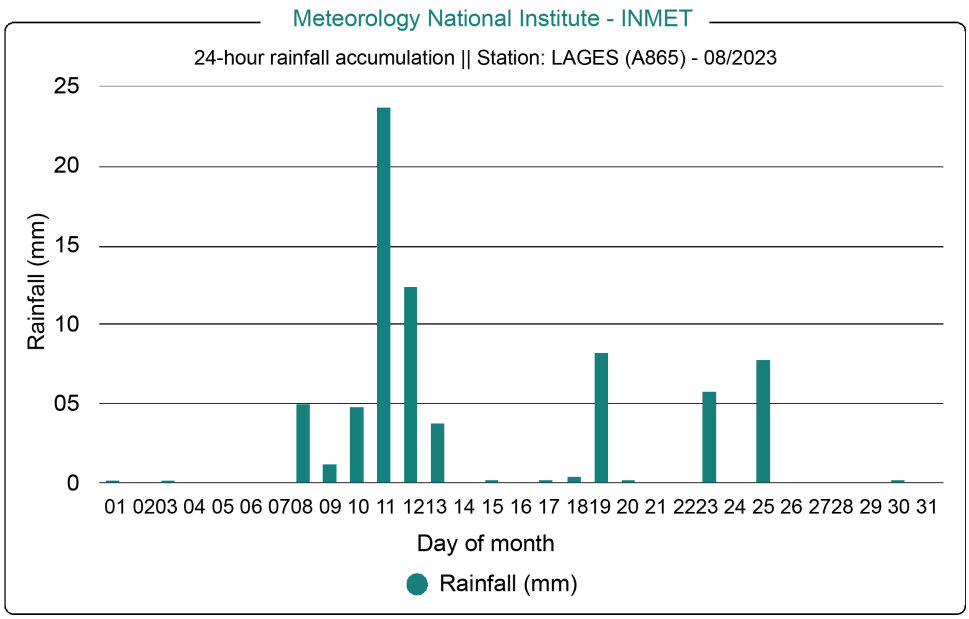

Figure 6. Rainfall in mm for the month of August 2023, winter collection period.

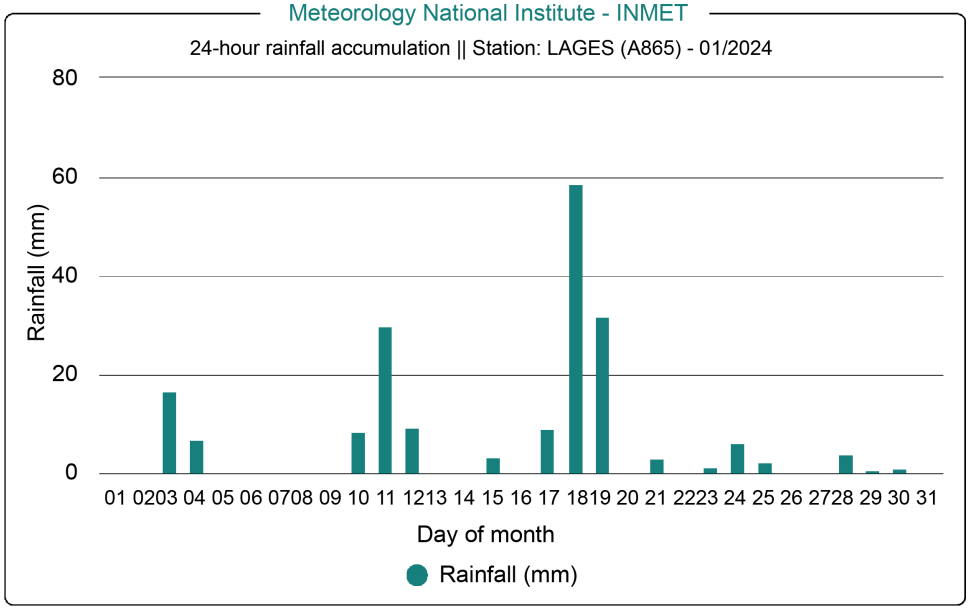

Figure 7. Rainfall in mm for the month of January 2024, summer collection period.

Table 4. Descriptive analysis of the collected data.

	Sodium	Potassium	Calcium	Magnesium	Chloride	Bicarbonate	Sulfate	EC	pH	Nitrate	Fluoride	Nitrite
Max	20.140	5.050	201.084	20.916	10.020	322	84.430	1217	9.300	6.170	1.950	-
Min	1.520	0.357	16.186	1.814	0.130	18	0.920	46.600	7	0.100	0.030	-
Mean	8.219	2.676	50.700	11.204	3.878	153.500	13.276	415.075	8.013	1.770	0.450	-
SD	6.591	1.648	28.044	6.954	4.055	92.642	28.840	351.631	0.781	2.512	0.656	-
CV	80%	62%	55%	62%	105%	60%	217%	85%	10%	142%	146%	-

Table 5. Ionic balance.

Sample	Na + K (meq/L)	Ca (meq/L)	Mg (meq/L)	Cl (meq/L)	CO_3 + HCO_3 (meq/L)	SO4 (meq/L)	EC (μS/cm)	Σ Cations (meq/L)	Σ Anions (meq/L)	I.B. I	I.B. II	Observations
P1 WINTER	0.093	0.360	0.149	0.012	0.295	0.065	46.600	0.602	0.372	47.160	23.580	Doesn't meet I.B. 2
P2 WINTER	0.954	2.919	0.781	0.054	3.081	0.034	298.000	4.655	3.169	37.970	18.990	Doesn't meet I.B. 1 and 2
P3 WINTER	0.367	4.439	1.721	0.264	3.639	0.135	473.000	6.526	4.038	47.110	23.550	Doesn't meet I.B. 1 and 2
P4 WINTER	0.471	3.159	0.934	0.029	2.590	0.030	245.000	4.564	2.649	53.100	26.550	Doesn't meet I.B. 1 and 2
P1 SUMMER	0.075	0.560	0.222	0.176	5.278	1.758	1217.000	0.857	7.211	157.500	78.750	Doesn't meet I.B. 1 and 2
P2 SUMMER	0.767	2.799	0.918	0.053	1.836	0.032	328.000	4.485	1.921	80.040	40.020	Doesn't meet I.B. 1 and 2
P3 SUMMER	0.297	3.479	1.658	0.283	2.032	0.138	471.000	5.434	2.453	75.590	37.800	Doesn't meet I.B. 1 and 2
P4 SUMMER	0.399	2.560	0.989	0.004	1.377	0.019	242.000	3.948	1.400	95.310	47.660	Doesn't meet I.B. 1 and 2

from the measured concentrations of selected analytes. The data reveal a substantial variation in values, as evidenced by the standard deviation (SD) and the coefficient of variation (CV), which indicate a notable dispersion of the data in relation to the mean. These indicators suggest a degree of heterogeneity in the hydrochemical composition of the sampled groundwater, possibly reflecting variations in the geological formations, aquifer characteristics, or anthropogenic influences at the sampling sites.

It is important to emphasize that nitrite concentrations were consistently found to be below the detection limit of the analytical method employed. As a result, statistical analysis for this parameter could not be performed, and it was excluded from the descriptive dataset.

Table 5 presents the ionic balance, in which ion concentrations originally expressed in milligrams per liter (mg/L) were converted to milliequivalents per liter (meq/L). This conversion enables the evaluation of the electrochemical balance between cations and anions in the water samples. Although none of the samples fell within the acceptable margin of error for ionic balance closure, values exceeding this threshold should not be disregarded. Such deviations may point to potential analytical or computational inaccuracies, the presence of minor ions not accounted for in the primary analysis, trace elements, or even naturally low mineralization levels in the sampled waters. These factors warrant careful consideration in the interpretation of hydrochemical data.

Regarding the cations (Na^+, K^+, Ca^{2+}, and Mg^{2+}), it was observed that sodium and potassium—two ions that are often strongly associated exhibited lower con-

centrations during the summer campaign compared to the winter, suggesting a dilution effect likely related to increased recharge. Calcium also showed a general dilution trend during the summer months relative to winter, with the exception of sample P1, where a subtle enrichment was noted. Magnesium levels were generally similar between both seasons; however, a slight enrichment was detected during the summer period, except in sample P3, which showed a dilution pattern. Figure 8 presents the graphical representation of the seasonal concentration variations for both cations and anions at the sampled locations.

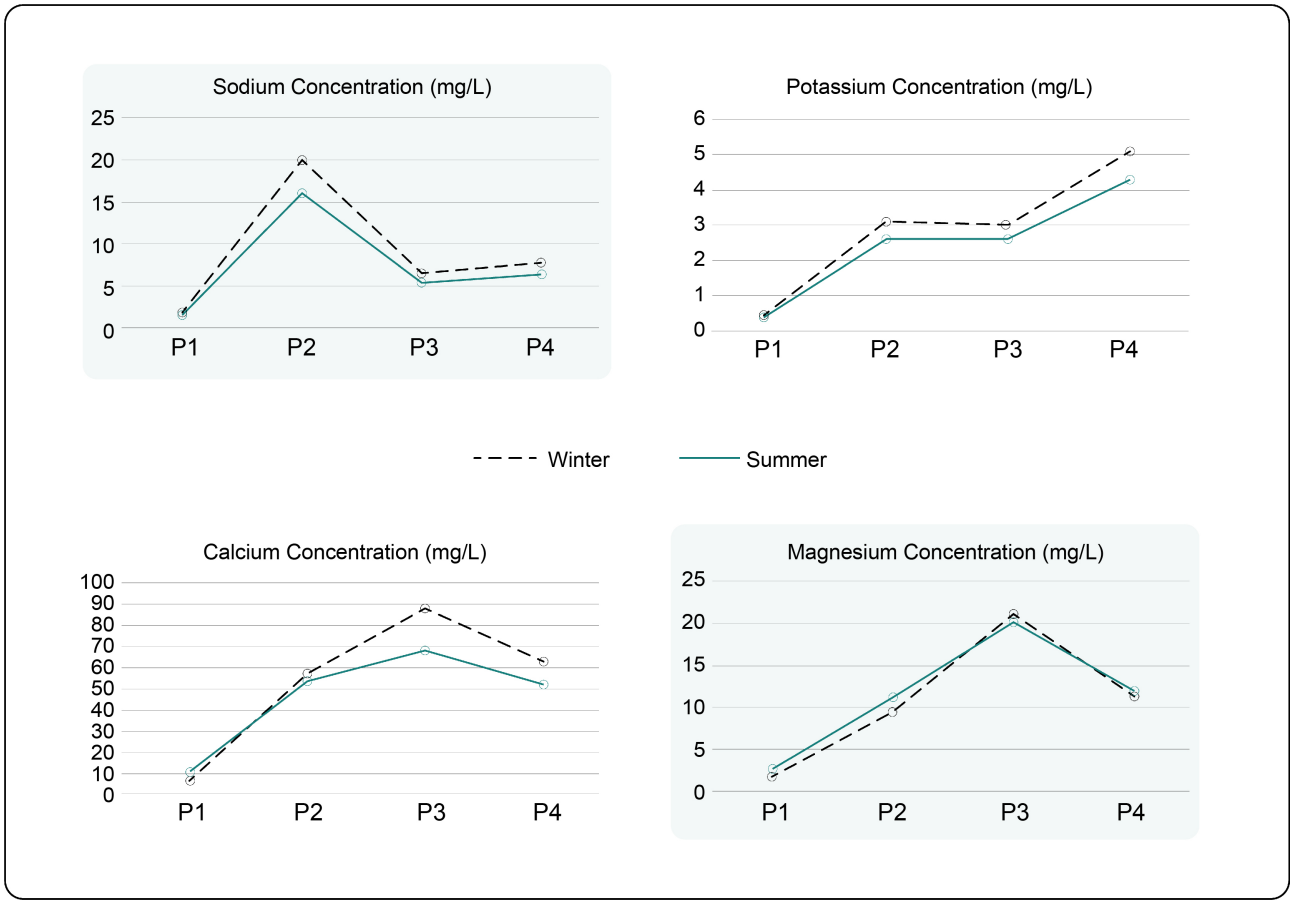

Figure 8. Cation graphs of the contents obtained in the winter and summer periods.

In terms of the anions analyzed (HCO_3^-, Cl^-, SO_4^{2-}, NO_3^-, NO_2^-, and F^-), a diffuse behavior was observed across the sampling periods, with both enrichment and depletion occurring depending on the ion and sampling point. Bicarbonate concentrations generally showed a decrease during the summer when compared to winter, except for sample P1, which exhibited an anomalous enrichment trend.

Chloride levels increased during the summer in samples P1 and P3, while samples P2 and P4 showed a slight dilution when compared to winter values. Sulfate concentrations were slightly higher in winter for samples P2 and P4; however, sample P3 exhibited an increase during the summer, and sample P1 again presented an anomalous enrichment during this same period.

Regarding nitrate, a general increase in concentration was observed during the summer, with the exception of sample P1, which experienced dilution. Nitrite concentrations in all samples remained below the minimum detection limit of the analytical equipment (0.03 mg/L) across both seasons. Lastly, fluoride exhibited a dilution trend during the summer, except for sample P1, which showed increased concentrations compared to the winter period (Figure 9).

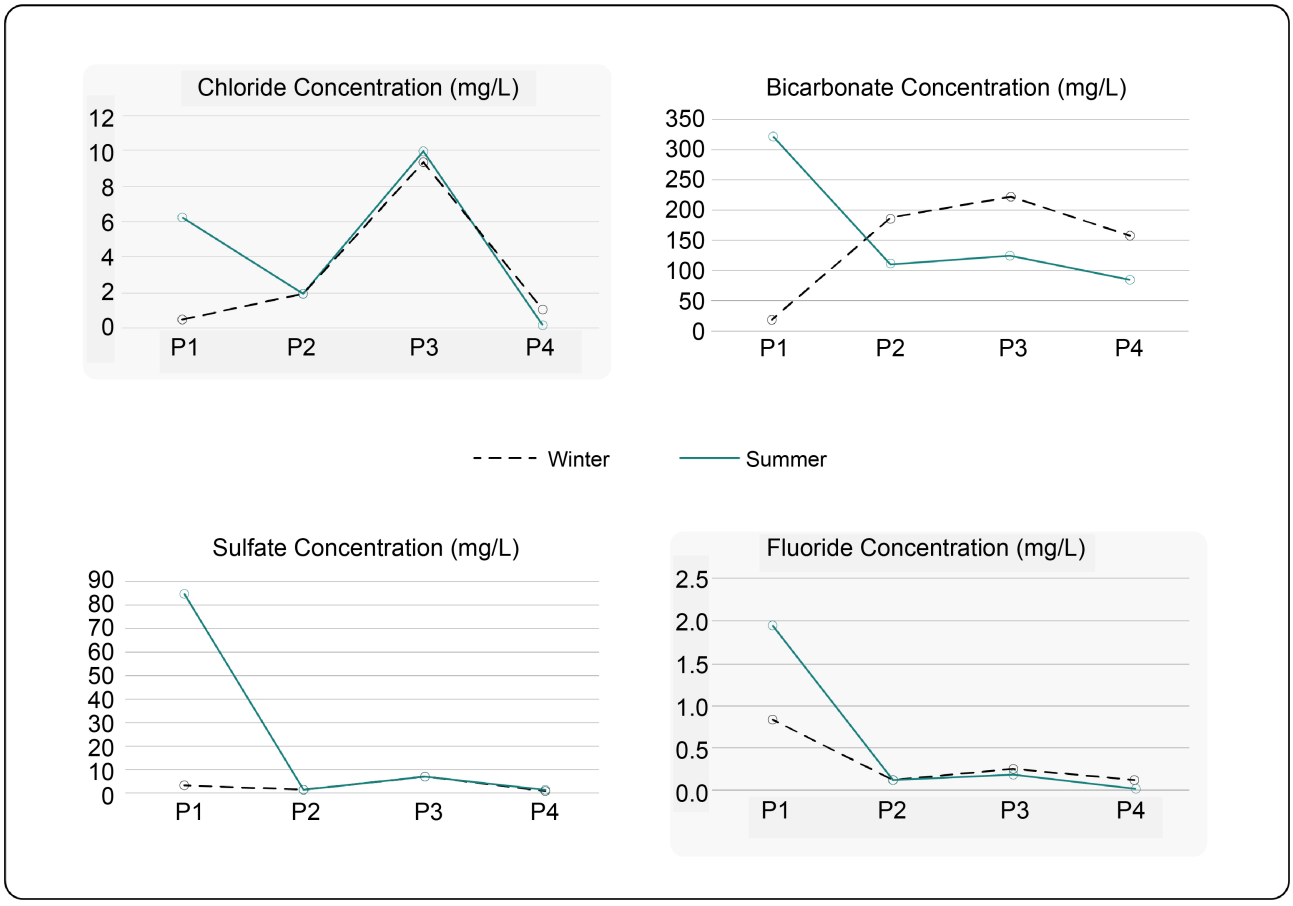

Figure 9. Graphs of the anions of the contents obtained in the winter and summer periods.

Regarding the total iron parameter in the samples, a dilution pattern was identified from the winter to the summer period. Based on the quantification of iron, it was observed that sample P1 exhibited a concentration exceeding 0.3 mg/L (0.3 ppm) in both sampling periods, rendering it non-potable according to both Brazilian and U.S. drinking water standards.

As for the Electrical Conductivity (EC) parameter, samples P2, P3, and P4 showed little variation between seasons. However, sample P1 exhibited low ionization during the winter sampling, with the opposite trend observed in the summer. This result aligns with the increased concentrations detected in sample P1 during the summer, indicating a general rise in solute content for this period.

In terms of pH, winter samples tended to exhibit values near neutrality, except for sample P1, which showed an alkaline character. In contrast, during the sum-

mer, all samples showed a shift toward alkalinity—particularly in samples P2, P3, and P4—while sample P1 exhibited a trend toward acidification, although it still retained an overall alkaline character (Figure 10).

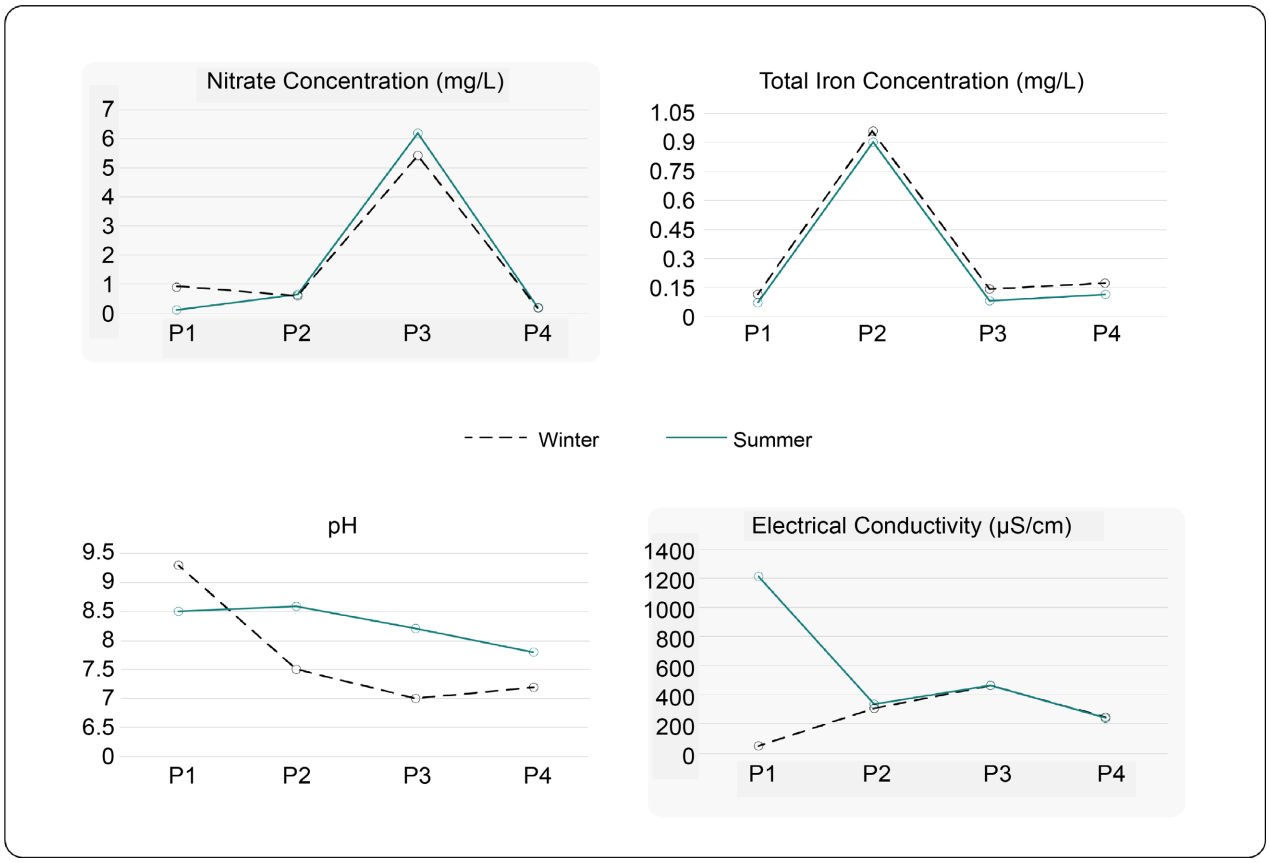

Figure 10. Analysis of the contents of Nitrate and Total Iron, Electrical conductivity and pH, in the winter and summer periods.

Regarding hydrochemical classification, all samples from the Rio do Rasto Formation, in both winter and summer, were classified within the calcium-magnesium bicarbonate facies, a trend commonly observed in unconfined aquifers. The results from the Piper diagram are consistent with the main ionic constituents of the samples, primarily calcium and bicarbonate (Figure 11).

When examining the anions on the diagram, samples P2 and P4 remained within the same field during both seasons. However, samples P1 and P3 exhibited variations within the bicarbonate facies. Sample P1, in winter, was positioned within the bicarbonate field but close to the chlorinated water field. During summer, an increase in the concentration of all ions was noted, with anomalous enrichment of bicarbonate and sulfate ions.

For sample P3, a depletion of bicarbonate and enrichment of chloride was observed. According to water classification, sample P2 essentially remained in the same area, showing only a slight increase in chloride concentration. A similar trend was observed for sample P3, but with a substantial increase in chloride levels.

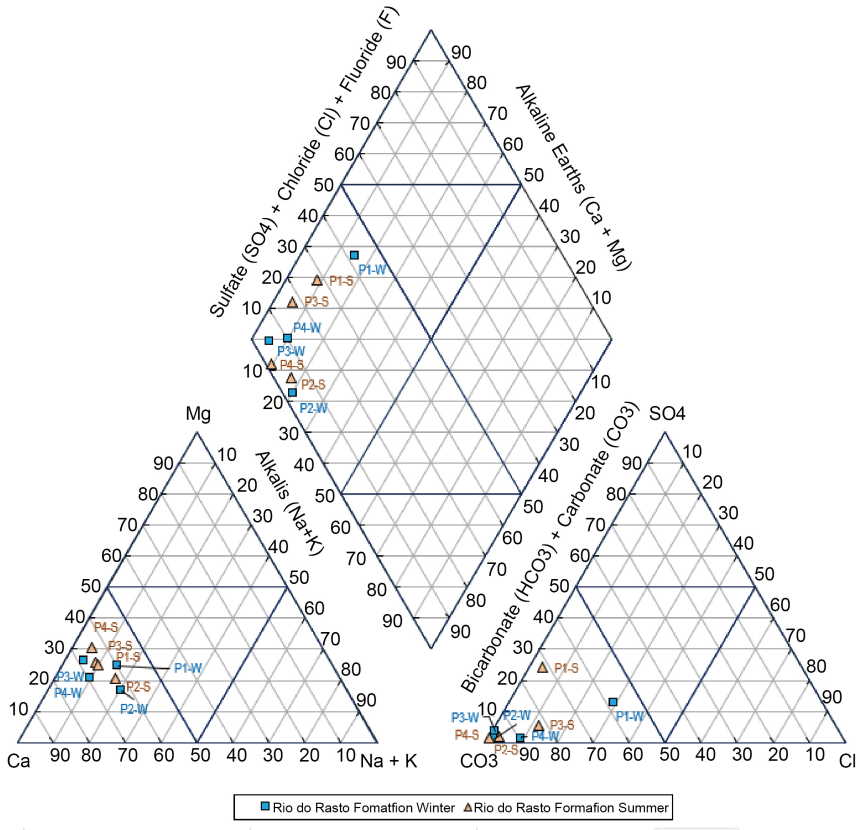

Figure 11. Results of the PIPER diagram.

Although all samples from the Rio do Rasto Formation remained within the calcium-magnesium bicarbonate facies, some variability within this hydrochemical facies was noted. Sample P1 showed depletion in winter, indicating characteristics suggestive of water mixing. However, during the summer sampling, a distinct calcium-magnesium bicarbonate signature was observed, possibly related to the high bicarbonate enrichment.

In sample P3, a depletion of dominant ions bicarbonate and calcium allowed other ions, particularly chloride, to have a greater influence.

The Schoeller diagram was constructed to observe the chemical signatures of samples from the Rio do Rasto Formation. The yellow line represents samples from P3, which showed virtually identical chemical signatures during both winter and summer, with minimal variation between seasons. A similar behavior is observed in the red line, representing samples from P2 (Figure 12).

The light blue line corresponds to sample P4, which, despite not coinciding exactly, exhibits the same overall trend: a pattern of chloride depletion followed by an increase in carbonate ions.

The samples that deviate from this pattern are those from P1, represented by the green line. During winter, this signature shows chloride depletion followed by a pronounced increase in sulfate and bicarbonate. In the summer, a similar trend is observed for cations, but this is followed by an increase in all anions.

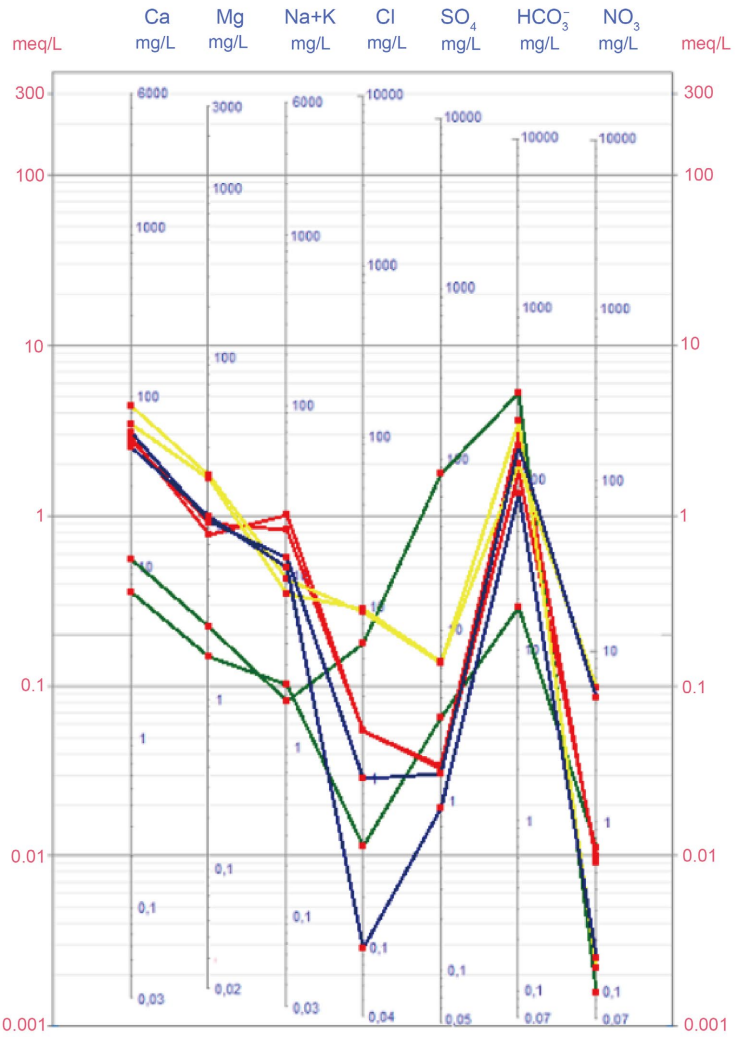

Figure 12. Schoeller diagram with the chemical signatures of the samples.

At first glance, these chemical signatures appear quite distinct. However, closer analysis reveals that they are quite similar, particularly regarding the pattern of cation depletion and anion increase. The primary factor causing this anomaly is the variable chloride content.

Several hypotheses could explain this behavior, but a plausible explanation is contamination by heterotrophic bacteria or the presence of fecal coliforms. As a remediation measure, well cleaning or disinfection is often performed using chlorine. The introduction of chlorine during this process may justify the anomalous increase in chloride concentration. Furthermore, this treatment may lead to the release of additional anions, as reflected in changes in pH. Although the sample pH remained alkaline, significant variations were observed alongside an increase in electrical conductivity (EC), highlighting the presence of available ions in the water.

When considering the local mineralogy, the observed hydrochemical behavior is consistent with the established data. The mineralogical composition primarily

includes quartz, feldspars, carbonates, and iron oxides. The Piper diagram indicates a calcitic mineral character, with localized dolomitic influence due to notable magnesium concentrations. This also suggests the presence of carbonate cement. Feldspars likely explain the relevant concentrations of sodium and potassium observed in the samples.

5. Conclusion

Based on the collected and analyzed data, the hydrochemical classification of samples from the Rio do Rasto Formation within the study area was established as predominantly calcium or magnesium bicarbonate types. These samples exhibit a behavior typical of unconfined aquifers, showing no evidence of significant water mixing, and are associated with a mineralogical composition characterized mainly by calcitic and locally dolomitic components. However, an examination of the stratigraphic profiles of the wells reveals that the interbedding of sand and fine-grained sediments suggests the behavior of a semi-confined aquifer system. In this context, the finer sediments likely act as sealing layers, restricting vertical water movement and contributing to the partial confinement of the aquifer. This observation supports the hypothesis that the area analyzed in this study may correspond to a semi-confined portion of the Rio do Rasto Formation.

The Schoeller diagram revealed a distinct chemical signature pattern among the samples. Although all samples belong to the same hydrochemical facies, they exhibit variations in their chemical signatures. Generally, the highest concentration peaks were observed for calcium, carbonate, and bicarbonate ions, alongside an overall trend of chloride depletionexcept for sample P1 during the summer season. Concentrations of magnesium, sodium, and potassium remained relatively stable across samples.

Regarding the sampling periods, summer recorded the highest rainfall, which generally resulted in dilution of ion concentrations, particularly cations. Anions also showed a subtle dilution trend, except for sample P1, which exhibited enrichment in all analyzed anions.

Analysis of ion concentrations and chemical signatures suggests that sample P1 experienced an anomalous increase in sulfate, likely linked to anthropogenic activities. It is worth noting that around the summer sampling period, the well was probably disinfected with chlorine, this assumption is based on the fact that the purpose of this well is exclusively dedicated to laundry activities, which generally require frequent cleaning procedures to maintain the well's performance. Otherwise, neglecting such maintenance may lead to issues such as the presence of bacteria, heavy metals, pesticides, and chemical residues. Additionally, total iron concentrations above the legal limits may be attributed to the natural geochemical characteristics of the Rio do Rasto Formation.

Acknowledgements

We extend our gratitude to all the laboratories that contributed to the analyses, to

FAPESC for their support, and especially to the Reservoir Geology Laboratory for their invaluable collaboration.

Conflicts of Interest

The authors declare no conflicts of interest regarding the publication of this paper.

References

Custódio, E., & Llamas, M. R. (1983). Groundwater Hydrology. *Omega, 1,* 157.

Edmunds, W. M., & Smedley, P. L. (1996). Groundwater Geochemistry and Health: An Overview. In J. D. Appleton, R. Fuge, & G. J. H. McCall (Eds.), *Environmental Geochemistry and Health* (pp. 91-105). British Geological Society Special Publication. https://doi.org/10.1144/gsl.sp.1996.113.01.08

Feitosa, F. A. C., Manoel Filho, J., Feitosa, E. C., & Demetrio, J. G. (2008). *Hydrogeology: Concepts and Applications* (3rd ed.). CPRM–LABHID.

Fenzl, N., & Ramos, J. F. (1986). *Introduction to Hydrogeochemistry*. Federal University of Pará.

Foster, S. S. D., & Chilton, P. J. (2003). Groundwater: The Processes and Global Significance of Aquifer Degradation. *Philosophical Transactions of the Royal Society of London. Series B: Biological Sciences, 358,* 1957-1972. https://doi.org/10.1098/rstb.2003.1380

França, A. B., Milani, E. J., Schneider, R. L., López, P. et al. (1995). Phanerozoic Correlation in Southern South America. *AAPG Memoir, 62,* 129-162.

Gordon, Jr. (1947). Classification of the Gondwana formations of Paraná, Santa Catarina, and Rio Grande do Sul. *Preliminary Notes and Studies DNPM-DGM, 38,* Article 20.

Hirata, R. C. A., Suhogußoff, A. V., Marcellini, S. S., Villar, P. C., & Marcellini, L. (2019). *Groundwater and Its Environmental and Socioeconomic Importance for Brazil* (1st ed.). Institute of Geosciences, University of São Paulo.

Holz, M., França, A. B., Souza, P. A., Iannuzzi, R., & Rohn, R. (2010). A Stratigraphic Chart of the Late Carboniferous/Permian Succession of the Eastern Border of the Paraná Basin, Brazil, South America. *Journal of South American Earth Sciences, 29,* 381-399. https://doi.org/10.1016/j.jsames.2009.04.004

Hounslow, A. (2018). *Water Quality Data: Analysis and Interpretation*. CRC Press.

Logan, J. (1965). *Interpretation of Chemical Analyses of Water*. U.S. Agency for International Development.

Machado, J. L. F. (2012). *Hydrogeological Map of the State of Santa Catarina. State Hydrogeological Maps, Water Availability Program in Brazil (Color Map, Scale 1:500,000)*. CPRM.

Menezes, J. M. et al. (2009). Water Quality and Its Spatial Relationship with Anthropogenic and Natural Contamination Sources: São Domingos River Watershed–RJ. *Agricultural Engineering, 29,* 687-698.

Milani, E. J. (1997). *Tectono-Stratigraphic Evolution of the Paraná Basin and Its Relationship with the Phanerozoic Geodynamics of Southwestern Gondwana*. Doctoral Thesis, Institute of Geosciences, Federal University of Rio Grande do Sul.

Milani, E. J., Gonçalves de Melo, J. H., de Souza, P. A., Fernandes, L. A., & França, A. B. (2007). Paraná Basin. *Petrobras Geosciences Bulletin, 15,* 265-287.

Rego, M. L. F. (1930). Petroleum Geology in the State of São Paulo. *Bulletin of the Geological and Mineralogical Service of Brazil, 46,* 1-105.

Rohn, R. (1994). *Environmental Evolution of the Paraná Basin during the Neopermian in Eastern Santa Catarina and Paraná*. Doctoral Thesis, Instituto de Geociências.

Rohn, R., Lages, L. C., & Penatti, J. R. R. (2003). Lithofacies of the Irati Formation in the FP-01-PR borehole (Permian, Eastern Border of the Paraná Basin). In *2nd Brazilian Congress on R & D in Petroleum & Gas* (pp. 52). CD-ROM.

Schneider, R. L., Mühlmann, H., Tommasi, E., Medeiros, R. A., Daemon, R. F., & Nogueira, A. A. (1974). Stratigraphic Review of the Paraná Basin. In *18th Brazilian Geological Congress* (pp. 41-65). SBG.

Soares, A. P., Soares, P. C., & Holz, M. (2008). Conflicting Stratigraphic Correlations at the Permo-Triassic Boundary in the Southern Paraná Basin: The Contact between Two Sequences and Implications for the Spatial Configuration of the Guarani Aquifer. *Research in Geosciences, 35,* 115-133.

State Secretariat for Sustainable Economic Development (2017). *State Water Resources Plan of Santa Catarina—Perh/Sc: General Characterization of the Hydrographic Regions of Santa Catarina—RH4 Planalto de Lages*.

Stollhofen, H., Stanistreet, I. G., Rohn, R., Holzförster, F., & Wanke, A. (2000). The Gai-As lake System, Northern Namibia and Brazil. In E. H. Gierlowski-Kordesch, & K. R. Kelts (Eds.), *Lake Basins through Space and Time* (pp. 87-108). AAPG.

Tolman, C. F. (1937). *Groundwater*. McGraw-Hill.

Tubbs Filho, D. (1994). *Hydrochemical Characterization and Vulnerability of Groundwater in the Coastal Region of the Municipality of Niterói, Rio de Janeiro State*. Master's Thesis, Federal Fluminense University.

Warren, L. V., Almeida, R. P., Hachiro, J., Machado, R., Roldan, L. F., Steiner, S. S., & Chamani, M. A. C. (2008). Sedimentary Evolution of the Rio do Rasto Formation (Permo-Triassic of the Paraná Basin) in the Central-Southern Portion of the State of Santa Catarina, Brazil. *Brazilian Journal of Geosciences, 38,* 213-227.

White, I. C. (1908). *Report on the Coal Measures and Associated Rocks in Southern Brazil*. Commission of Coal Mines of Brazil.